Hindawi
Wireless Communications and Mobile Computing
Volume 2022, Article ID 5772168, 13 pages
https://doi.org/10.1155/2022/5772168

Research Article

A Novel Method for Diagnosis of Broken Bars Based on Optimum Resolution of Prescient Direction Algorithm

Zhuzhi Jia,[1] **Yizhe Wang**,[2] **Hongyu Zhu**,[2] **and Xiangjin Song**[3]

[1]*School of Applied Technology, University of Science and Technology Liaoning, Anshan, Liaoning 114051, China*
[2]*School of Electronics and Information Engineering Department, University of Science and Technology Liaoning, Anshan, Liaoning 114051, China*
[3]*School of Electrical and Information Engineering, Jiangsu University, Zhenjiang, Jiangsu 212013, China*

Correspondence should be addressed to Zhuzhi Jia; jiazhuzhi@ustl.edu.cn

Received 25 April 2022; Revised 10 June 2022; Accepted 24 June 2022; Published 15 July 2022

Academic Editor: Kuruva Lakshmanna

Fourier transformation (FT) and Multiple Signal Classification (MUSIC) method suffer the insufficient ability in diagnosing broken rotor bar (BRB) fault using short-time data. Theoretical and simulation analyses show that the Optimum Resolution of Prescient Direction (ORPD) algorithm has the best frequency resolution performance due to a priori knowledge. The main objective of this paper is to detect BRB faults in induction machines using a condition monitoring architecture based on ORPD algorithm. In the proposed application, the ORPD algorithm with the best frequency resolution performance is used to estimate the fault-sensitive frequencies in the stator current signature. The prior information of BRB fault characteristic distribution is used to construct a weighting matrix in the ORPD algorithm, for acquiring the lowest signal-to-noise ratio resolution threshold. Once frequencies are estimated, their corresponding amplitudes are obtained by using the least squares estimator. The proposed methods were tested using experimental induction motors with different fault severity under the effect of several load levels or supply frequencies. Two types of power supply modes are considered: main and inverter. The results show that compared with traditional method which uses FT and MUSIC algorithm for fault diagnosing, the method based on ORPD algorithm has a higher frequency resolution and identification ability with short-time data, and still has good diagnostic performance even under light loading and lower supply frequencies.

1. Introduction

Squirrel cage induction motors are the most common way of electro-mechanical energy conversion in the main industrial applications. Traditionally, induction motors were conceived as robust machines. However, due to the fact that induction motors often operate in unwanted conditions such as corrosive place and misoperations, the probability of a fault increases, even more since inverters are used to drive the motor. Among the various faults, broken rotor bars (BRBs) account for about 10% of total failures. Induction motor faults such as BRBs can result in potential physical damage to motor itself as well as to the reliability and safety of industrial operations, and also increase the operational costs [1–3]. Therefore, induction motor condition monitoring and fault diagnostics have created substantial interest among researchers in the last decades, and many of them are with great respect to BRB detection.

Motor Current Signature Analysis (MCSA) is a widely adopted technique for online diagnostics of BRBs in motor. It has been demonstrated that BRBs produce additional spectral components in the stator current spectrum around the fundamental, with frequencies given by $f_b = (1 \pm 2s)f_s$, which s is the slip and f_s is the fundamental frequency. The frequency location of these components is associated with the slip s and the fundamental frequency f_s. The severity of BRB is indicated by the magnitude of the fault component [4–6]. In Fourier transform (FT) based MCSA, the spectrum of stator currents can be used to diagnose BRB faults in motors. FT yields computationally efficient results, which makes it a powerful and conceptually simple MCSA technique. Despite these advantages, its validity has some

drawbacks when the approach is applied under certain conditions. In practical industrial applications, the two BRB frequency components are very close to the fundamental frequency in a light load condition. This requires the data points used for FT to be long for sufficient frequency resolution, but it is not always possible due to the limitation of the digital system memory size. Moreover, short data records are usually required because the motor operating condition may change during the recording period, which makes diagnostic indicators changing with the motor load and application of MCSA impossible. In BRB fault diagnosis, the problem of frequency estimation using much shorter data windows to satisfy the same frequency resolution requirement, and gaining a higher accuracy of frequency estimation using the same length windows has received a lot of attention in the electrical engineering community [3, 7–9].

In order to improve the diagnostic performance of FFT-based methods, signal windowing, frequency interpolation, ZFFT techniques, and maximum covariance method for frequency tracking (MCFT) to compute the frequency of the fault signature have been reported. All the above methods emphasize the compromise between frequency accuracy, frequency resolution, and computation time of frequency estimation for BRBs detection in induction motors [10, 11]. Furthermore, nonparametric and parametric techniques are employed to the BRBs detection taking into account the fact that the signal of stator current is nonstationary. Unfortunately, the nonparametric methods exist same frequency resolution problems compared to the classical FFT-based methods. To overcome these issues, diverse parametric techniques such as the Prony and Pisarenko approaches have been developed for frequency estimation. Due to the fact that frequency estimation and direction of arrival (DOA) estimation are essentially the same, the Multiple Signal Classification (MUSIC) method, which is the main branch of DOA estimation, has also been introduced in the area of BRB fault detection [11–16]. MUSIC method transforms the fault detection problem into a generalized eigenvalue problem by calculating the current signal self-correlation matrix and eigenvalue decomposition. MUSIC method uses smaller samples of measured data and has a higher frequency resolution than FT. However, in a real application, the high resolution of MUSIC method is at the expense of increasing the computing time, and the accuracy depends on the dimension of the autocorrelation matrix. In addition, amplitude estimation is still required, because the MUSIC method is a pseudo-spectrum estimation, which cannot reflect the amplitude of fault characteristic frequency [14]. In [17], the authors have analyzed the influence of the dimension of self-correlation matrix and sampling rate on the performance of MUSIC method. In [18], Akaike information criterion (ACI) and minimum description length (MDL) criterion have been used to optimize the dimension M of the self-correlation matrix, so as to minimize the operation time. In [11], an algorithm that is based on zooming in a specific frequency range is proposed with MUSIC. The method is integrated as a part of MUSIC to estimate the frequency signal dimension order based on classification of autocorrelation matrix eigenvalues. An application of the MUSIC and the pattern search algorithm (PSA) has been proposed to detect BRB fault in induction motors with short-time measurement data in [19]. In the above-mentioned researches [11, 16, 19], the data time used for BRB fault diagnosis is shortened to 1.5 s, and good diagnostic results can be achieved if the workload is already at or near 40% rated loads.

Although MUSIC algorithm has good frequency estimation performance, its application is constrained to just specific noncorrelated signals. For related signal or the signal with low signal-to-noise ratio (SNR), the frequency estimation performance gradually deteriorates [20]. In practical applications, detecting BRB in a light load condition especially for the inverter-fed motor running under low-frequency band is yet challenging as the fault frequency components are very close to the fundamental and have low amplitude. In [21, 22], analysis is made on statistical performance of MUSIC-type high-resolution estimators. Factors affecting its proper use and approaches for improvement are discussed. Based on the concept of statistical average value of zero spectrum, the resolution performance for all varieties of eigen-structure approaches, including MUSIC algorithm, is compared and analyzed in [23–25], and the formulation results of SNR thresholds to resolve two incorrelated equal power signal for several typical eigen-structure approaches are given. The above research reveals the fundamental flaws that limit the improvement of frequency resolution of MUSIC algorithm and shows that under certain conditions, algorithms with different frequency resolutions can be obtained by changing the distribution structure of eigenvalues and the spatial projection relationship.

In principle, Optimum Resolution of Prescient Direction (ORPD) algorithm and MUSIC all belong to the eigen-structure approaches. With different feature vector space projection relationship of self-correlation matrix, they correspond to different algorithm structure and frequency resolution performance. For two unknown signals whose direction angles are θ_1 and θ_2, ORPD algorithm uses the prior information of the known intermediate point θ_m to estimate the parameters, which can realize the high-precision identification of the direction angle θ and thus has the best frequency resolution performance. The ORPD algorithm is mainly used for radar low-angle tracking in the field of direction estimation of wave arrival [24, 25]. Nevertheless, the authors have not found in the literature any application of this tool for the diagnosis of electrical machines. When BRB fault occurs, the frequency components $(1 \pm 2\,\mathrm{s})f_s$ are symmetrically distributed on the two sides of the fundamental frequency f_s. This characteristic is naturally consistent with the application conditions of ORPD algorithm, which provides an idea for the development of a new diagnosis method.

The aim of this paper is to introduce a new high-resolution ORPD algorithm and its application for detecting BRB fault diagnosis by the frequency domain analysis. The suitability of this diagnostic tool is experimentally tested in the diagnosis of BRBs in main-fed as well as inverter-fed squirrel cage induction

motors with different conditions of load and fault severity. The proposed ORPD estimator can precisely determine the BRB fault-sensitive frequencies. By using the prior knowledge of the intermediate point of BRB fault characteristic frequencies, a weighted matrix which can obtain the minimum SNR resolution threshold is constructed. Thus, the ORPD algorithm with the best frequency resolution performance is formed to estimate the frequency. Due to the fact that BRB fault characteristic frequencies given by $f_b = (1 \pm 2\,\mathrm{s})f_s$ are distributed across low-frequency band, filtering technique is used to confine the analysis to the frequency band related to the characteristic frequencies to improve SNR and reduce the computation load. Once the frequency estimation has performed, their corresponding amplitudes are obtained by least squares (LS). Finally, diagnostic decision is made.

The main contributions of this paper can be summarized as follows.

(1) The eigen-structure approaches are hopeful to be able to provide even better resolution performance if more a priori information about the characteristic frequencies is utilized sufficiently. In MUSIC and its extensions, model order estimation techniques based on the eigenvalue decomposition of the covariance matrix are proposed to improve resolution performance. However, these eigenvalue-based techniques do not exploit the particular structure of the stator current frequency components. In this paper, we use the midpoint frequency of BRB fault characteristic frequencies to construct weighted matrix, which can obtain the minimum SNR resolution threshold. The resulting technique exhibits high-resolution capabilities

(2) We prove the effectiveness of the technique on simulated and experimental data. Compared with available FT and MUSIC methods, the proposed method has the advantages of less required data, high-frequency resolution, short running time, and wide diagnostic range. Experimental results show that the proposed method only needs 1 s of short-time data to complete the diagnosis of BRB faults under different power supply modes and different operating conditions, and still achieves good diagnosis result under 20% load

The remainder of this paper is organized as follows. Section 2 describes the theoretical basis of eigen-structure approach based frequency estimation and the feasibility and performance of ORPD algorithm for BRB fault diagnosis. Section 3 gives the proposed diagnosis method and experimental setup. Section 4 shows the experimental results for the BRB fault. Section 5 concludes this paper.

2. Theoretical Basis of Frequency Estimation

2.1. Basic Principle of Parameter Estimation by Eigen-Structure Approach. The eigen-structure approach assumed a priori signal model seeks to fit a deterministic exponential model to equally spaced data points. It was discussed in detail by Pillai [21] and Kaveh [22]. Here we will give a brief review of this technique. Consider discrete time signals

$$x[n] = s[n] + e[n] = \sum_{i=1}^{K} a_i \cos\left(2\pi f_i n + \varphi_i\right) + e[n], \quad (1)$$

where $s[n]$ is the sum of K sinusoidal quantities, $e[n]$ is white noise with zero mean and σ^2 variance, and a_i, f_i, and φ_i are the amplitude, frequency, and phase of the i-th sinusoid, respectively. Using Euler's transformation, Equation (1) can be expressed in the form of a complex exponential as shown in Equation (2).

$$x[n] = s[n] + e[n] = \sum_{i=1}^{M} \bar{A}_i e^{j2\pi \bar{f}_i n} + e[n], \quad (2)$$

where $s[n] = \sum_{i=1}^{M} \bar{A}_i e^{j2\pi \bar{f}_i n}$, $\bar{A}_i = (a_i/2)e^{j\varphi_i}$, $\bar{A}_{K+i} = (a_i/2)e^{j\varphi_i}$, $\bar{f}_i = f_i$, $\bar{f}_{K+i} = -f_i$, $1 \le i \le K$, and $M = 2\,\mathrm{K}$.

The i-th complex sinusoid is defined as $s_i(n) = \bar{A}_i e^{j2\pi \bar{f}_i n}$, and Equation (2) can be written as:

$$x[n] = \sum_{i=1}^{M} s_i(n) + e[n]. \quad (3)$$

For L-dimensional discrete time series $\{x[n], x[n+1], \cdots, x[n+L-1]\}$, Equation (3) can be rewritten in a compact matrix format as shown in Equation (4).

$$\mathrm{X}[n] = \sum_{i=1}^{M} \mathrm{S}_i(n) + \mathrm{e}[n] \quad (4)$$

where $L > M$, $\mathbf{X}(n) = [x[n], x[n+1], \cdots, x[n+L-1]]^T$, $\mathbf{S}_i(n) = [s_i[n], s_i[n+1], \cdots, s_i[n+L-1]]^T$, $\mathbf{e}(n) = [e[n], e[n+1], \cdots, e[n+L-1]]^T$。

Where the i-th complex sine vector $\mathbf{S}_i(n)$ can be expressed as,

$$\mathrm{S}_i(n) = \begin{bmatrix} s_i[n] \\ s_i[n+1] \\ \vdots \\ s_i[n+L-1] \end{bmatrix} = \begin{bmatrix} 1 \\ e^{j2\pi \bar{f}_i} \\ \vdots \\ e^{j2\pi \bar{f}_i (L-1)} \end{bmatrix} \bar{A}_i e^{j2\pi \bar{f}_i n}. \quad (5)$$

Substituting Equation (5) into Equation (4), the low-rank matrix representation of the eigen-structure approach is obtained as shown in Equation (6).

$$\mathrm{X}[n] = \mathrm{F}\bar{\mathrm{A}} + \mathrm{e}[n], \quad (6)$$

where $\mathrm{F} = [\mathrm{f}(\bar{f}_1), \mathrm{f}(\bar{f}_2), \cdots, \mathrm{f}(\bar{f}_M)]$, $\mathrm{f}(\bar{f}_i) = [1, e^{j2\pi \bar{f}_i}, \cdots, e^{j2\pi \bar{f}_i (L-1)}]^T$, $i = 1, 2, \cdots, M$, $\bar{\mathrm{A}} = [\bar{A}_1 e^{j2\pi \bar{f}_1 n}, \bar{A}_1 e^{j2\pi \bar{f}_2 n}, \cdots, \bar{A}_M e^{j2\pi \bar{f}_M n}]^T$. $\mathbf{F}$ is an M order $L \times M$

Vandermonde matrix, $\mathrm{f}(\bar{f}_i)$ is the signal vector with parameter $\bar{f}_i$.

The self-correlation matrix $\mathbf{R}_x$ of measured data $\mathrm{X}(n)$ can be expressed as:

$$R_{\mathrm{x}} = E\left[X(n)X^H(n)\right] = \mathrm{F}\mathrm{R}_{\bar{\mathrm{A}}}\mathrm{F}^H + \sigma^2\mathrm{I}_L, \tag{7}$$

where $\mathbf{E}[\cdot]$ is the mathematical expectation, $\mathrm{R}_{\bar{\mathrm{A}}} = E[\bar{\mathrm{A}}\,\bar{\mathrm{A}}^H]$ is the signal correlation matrix, $\mathbf{I}_L$ is an $L \times L$ identity matrix.

The eigenvalues of the self-correlation matrix $\mathbf{R}_x$ and $\hat{\mathrm{R}}_x$ are decomposed into:

$$R = \sum_{i=1}^{L} \lambda_i e_i e_i^H ; \hat{R} = \sum_{i=1}^{L} \hat{\lambda}_i \hat{e}_i \hat{e}_i^H, \tag{8}$$

where the subscripts of all eigenvalues and eigenvectors are arranged according to the order of size, namely, $\{\lambda_1 \geq \lambda_2 \geq \cdots \geq \lambda_L\}$ and $\{\boldsymbol{e}_1, \boldsymbol{e}_2, \cdots, \boldsymbol{e}_L\}$. If rank $(\mathbf{R}_x) = \mathrm{M}$, the following eigenvalues can be obtained:

$$\lambda_1 \geq \lambda_2 \geq \cdots \geq \lambda_M > \lambda_{M+1} = \lambda_{M+2} = \cdots = \lambda_L = \sigma^2. \tag{9}$$

Using the eigenvectors of Equation (9) and $\mathbf{R}_x$, the signal subspace matrix $\boldsymbol{E}_S = [\boldsymbol{e}_1, \boldsymbol{e}_2, \cdots, \boldsymbol{e}_M]$ and the noise subspace matrix $\boldsymbol{E}_N = [\boldsymbol{e}_{M+1}, \boldsymbol{e}_{M+2}, \cdots, \boldsymbol{e}_L]$ with eigenvalues σ^2 are defined, where estimated matrices for $\boldsymbol{E}_\mathrm{S}$ and $\boldsymbol{E}_\mathrm{N}$ are $\hat{E}_S = [\hat{e}_1, \hat{e}_2, \cdots, \hat{e}_M]$ and $\hat{E}_N = [\hat{e}_{M+1}, \hat{e}_{M+2}, \cdots, \hat{e}_L]$, respectively. Accordingly, the signal subspace estimation $\hat{S}_q^L = \mathrm{span}\{\hat{e}_1, \hat{e}_2, \cdots, \hat{e}_q\}$ and noise subspace estimation $\hat{N}_{Lq}^L = \mathrm{span}\{\hat{e}_{M+1}, \hat{e}_{M+2}, \cdots, \hat{e}_L\}$ can be obtained.

The basic idea of eigen-structure approach is to estimate the value of signal parameter $\bar{f}_i$ by using the relationship between the signal subspace of signal vector $\mathrm{f}(\bar{f}_i)$ and each characteristic vector. Constructing the search function as shown in Equation (10) and searching the projection of $\mathrm{f}(\bar{f}_i)$ on $\hat{N}_{L-q}^L$, the estimated value of the parameter $\bar{f}_i$ $(i = 1, \cdots M)$ can be obtained, according to the value of $\bar{f}$ that minimizes the projection modulus (the position of the peak).

$$\hat{\alpha}(\bar{f}) = \frac{\mathrm{f}^H(\bar{f})\mathrm{f}(\bar{f})\mathrm{tr}[\hat{\mathrm{W}}]}{\mathrm{f}^H(\bar{f})\hat{E}_N\hat{\mathrm{W}}\hat{E}_N^H\mathrm{f}(\bar{f})}. \tag{10}$$

2.2. Frequency Estimation Based on ORPD Algorithm. The resolution performance of the eigen-structure approach refers to the ability to separate signals with similar parameters on the "spectrum." When calculating the self-correlation matrix $\mathbf{R}_x$ according to Equation (8), the self-correlation matrix of the sample is used to replace the real self-correlation matrix. Therefore, there must be errors between the eigenvalues and eigenvectors obtained by eigenvalue decomposition of $\mathbf{R}_x$ and their real values. Statistical analysis of the eigenvalues and eigenvectors of the $\mathbf{R}_x$ matrix shows [21–23] that the resolution performance of the zero spectral parameter estimation obtained according to Equation (10) is related to the weighted matrix $\boldsymbol{W}$ and SNR. In order to obtain the eigen-structure approach with the best resolution performance, two signals with very close frequencies f_1 and f_2 are considered, and $f_m = (f_1 + f_2)/2$ is assumed to be the intermediate value of the two frequencies. The SNR's resolving threshold of parameter estimation by the eigen-structure approach is defined as the SNR satisfying Equation (11).

$$D(\bar{f}m) = \frac{D(\bar{f}1) + D(\bar{f}2)}{2}, \tag{11}$$

where $D(\bar{f}) = \mathrm{E}\{\hat{D}(\bar{f})\} = \mathrm{E}\{\mathrm{f}^H(\bar{f})\hat{E}_N\hat{W}\hat{E}_N^H\mathrm{f}(\bar{f})\}$.

It has been proved [23] that for the eigen-structure zero-spectrum estimation Equation (10) with complex Emmett weighting matrix $\boldsymbol{W}$, when the weighting matrix $\boldsymbol{W}$ has the form of Equation (12), the lowest SNR's resolving threshold $\boldsymbol{\xi}_T$ can be obtained, and the unidentifiable frequencies f_1 and f_2 can be distinguished.

$$\boldsymbol{W} = \boldsymbol{E}_N^H e(f_m)e^H(f_m)\boldsymbol{E}_N, \tag{12}$$

$$\xi_T = 20\frac{1 + \sqrt{1 + N\Delta^2(1\text{-}4/L^2)/5}}{LN\Delta^4(1\text{-}4/L^2)(1\text{-}1/L^2)}. \tag{13}$$

In Equation (13), N is data length, L is signal dimension, and Δ is signal distance. Consequently, the ORPD algorithm based parameter estimation equation is shown in (14).

$$\hat{\alpha}(f) = \frac{f^H(f)f(f)\mathrm{tr}\left[\hat{E}_N^H f(f_m)f^H(f_m)\hat{E}_N\right]}{f^H(f)\hat{E}_N\hat{E}_N^H f(f_m)f^H(f_m)\hat{E}_N\hat{E}_N^H f(f)}. \tag{14}$$

In practice, f_m is usually unpredictable. In this case, the weighted matrix can be constructed by assuming that f_m follows a certain probability distribution and then taking the average value. Both MUSIC and mini-norm algorithm are all special cases of this processing method, in which the f_m is assumed that uniformly distribute in the interval of $(0 \sim 2\pi)$. The resolution performance based on the above hypothesis is not optimal, but can only get suboptimal effect. For BRBs failure, the characteristic frequencies $(1 - 2s)f_s$ and $(1 + 2s)f_s$ are distributed on the left and right sides of the fundamental frequency f_s, and their middle frequency f_m can be accurately known. Consequently, the weighted matrix W that meets the minimum SNR resolution threshold can be accurately obtained, and the ORPD algorithm obtained on this basis has a higher frequency resolution. So accurate estimation of the characteristic frequencies of BRBs $(1 - 2s)f_s$ and $(1 + 2s)f_s$ can be achieved.

2.3. Amplitude Estimation. The pseudo-power spectrum obtained by Equation (14) cannot provide the amplitude of the corresponding frequency component. Using the estimation matrix $\hat{\mathrm{F}}$ in Equation (6), the least square method is adopted to design the LS amplitude estimator as shown in Equation (15). Then, according to Euler's formula, the amplitude estimate $\hat{a}_i$ corresponding to the frequency

estimate $\widehat{f}_i$ can be obtained by taking the absolute value of $\widehat{\widehat{\mathrm{A}}}$, $1 \le i \le K$.

$$\widehat{\widehat{\mathrm{A}}} = \left(\widehat{\mathrm{F}}^H \widehat{\mathrm{F}}\right)^{-1} \widehat{\mathrm{F}}^H x_T(n), \tag{15}$$

where $\boldsymbol{x_T(n)} = [x[n], x[n+1], \cdots, x[n+N-1]]^T$.

2.4. Simulation Results. The performance of the proposed ORPD algorithm is evaluated in Matlab in terms of its resolvability of closely spaced sinusoids. The aim of this section is to highlight the high-resolution performance of ORPD algorithm compared classic MUSIC method. Three synthetized signals $i_1(t)$, $i_2(t)$, and $i_3(t)$ were considered, composed of only two harmonic components, respectively.

$$i_1(t) = \cos\left(2\pi \cdot 49.3 \cdot t + 0.23\pi\right) + \cos\left(2\pi \cdot 50.7 \cdot t + 0.3\pi\right), \tag{16}$$

$$i_2(t) = \cos\left(2\pi \cdot 49.4 \cdot t + 0.23\pi\right) + \cos\left(2\pi \cdot 50.6 \cdot t + 0.3\pi\right), \tag{17}$$

$$i_3(t) = \cos\left(2\pi \cdot 49.5 \cdot t + 0.23\pi\right) + \cos\left(2\pi \cdot 50.5 \cdot t + 0.3\pi\right). \tag{18}$$

In all cases, the signals were sampled at the frequency of 2 kHz during 1 s, white Gaussian noise was added, SNR was set to 20 dB, and dimension M of self-correlation matrix was set to 100.

The pseudo-spectra of MUSIC and ORPD corresponding to signal $i_1(t)$, $i_2(t)$, and $i_3(t)$ are shown in Figure 1. The observed pseudo-spectra integrate the statistical results of 20 simulation experiments.

As shown in Figure 1, under the same conditions such as SNR, data length N, and matrix dimension M, the resolution performance of ORPD and MUSIC algorithm varies with the change of frequency interval. In Figure 1(a), when the two frequency components are far away from each other, the resolution of MUSIC and ORPD algorithms is roughly equal. However, when the two frequency components gradually approach each other, the resolution of MUSIC algorithm begins to decline, as shown in Figure 1(b). The spectral peak of MUSIC algorithm is ambiguous, while ORPD algorithm still maintains high resolution. When the two frequency components are very close to each other, as shown in Figure 1(c), there is only one spectrum peak and cannot identify two frequencies by MUSIC algorithm, but still two spectrum peaks clearly by ORPD algorithm. So ORPD algorithm can still distinguish two closely spaced sinusoid frequencies. By averaging each result of the ORPD algorithm in Figure 1(c), the left and right frequency values are 49.52 Hz and 50.53 Hz, respectively. Within the allowable error range, the frequency values obtained by ORPD algorithm are very close to the real frequency, indicating that ORPD algorithm has higher resolution performance and can accurately distinguish two signals with very similar frequency values. The simulation results show that ORPD algorithm can be used for broken rotor bar fault diagnosis and has higher frequency resolution than MUSIC algorithm. Many pseudo peaks will be generated when ORPD algorithm is used, and the spectral peaks in the stopband processed by band-pass filtering can be identified as "pseudo peaks" and excluded.

3. Experimental Setup

The general view of the experimental setup is depicted in Figure 2. The test motor used in the experimental investigation is a three-phase, 50 Hz, 4-pole, 3 kW, 380 V, 6.8A, Y-connected induction motor. Several identical type rotors with different broken bars, which can be interchanged, have been prepared for testing. Each of them is a standard cast aluminum single-squirrel cage-type rotor with 32 skewed and uninsulated bars. The broken rotor bar fault is constructed by drilling holes through the rotor bars at the joints with the end ring using a fine milling cutter. An industrial drive (Siemens, 6SE6440-2UD31-8DB1) has been employed to apply open-loop constant voltage/frequency (CV/F) control technique for the different operating conditions. A three-phase change-over switch is used for exchanging the motor connection from the mains to the drive output and vice versa. A separately excited 4 kW DC generator with a variable resistance box is used as the load of the motor. The current signal is acquired by using a current transducer with a data acquisition card during 10s. The sampling frequency is 2 kHz.

The tests are performed with the motor in different steady-state regime. First, the motor is in healthy condition. In the second group of tests, the motor is the utility-driven case and the supply frequency is 50 Hz. During the experiment, the load is adjusted randomly to make the motor run under 20%, 23%, 25%, 50%, and 75% rated load, respectively. The third group of tests corresponds to the same motor with inverter-driven cases. Contrary to the utility-driven case, in CV/F mode, the motor reference frequency is adjustable. Therefore, the low supply frequencies of 20 Hz, 32 Hz, 40 Hz, and 45 Hz are investigated. Data acquisition is done via National Instruments NI USB6216, LEM LA55-P current probe, and standard PC notebook computer. The signal processing software has been implemented by using the MATLAB R2014a on a PC processor, having Intel(R) Core(TM) i5-4300U CPU, and 64-bit Windows 7 operating system.

The proposed fault detection methodology is summarized in Figure 3. First of all, the captured single-phase current signal is filtered in order to suppress frequency components, related to the fundamental component as well as other stator winding harmonics. This procedure, which yields a clearer representation of the results, is applied gradually, eliminating the main current harmonic in all cases and removing higher order ones as needed. Chebyshev notch filter and Batworth 4-order band-pass filter, as implemented in MATLAB, are suitable for this task. The filter preprocessing overcomes the problems of judging the number of

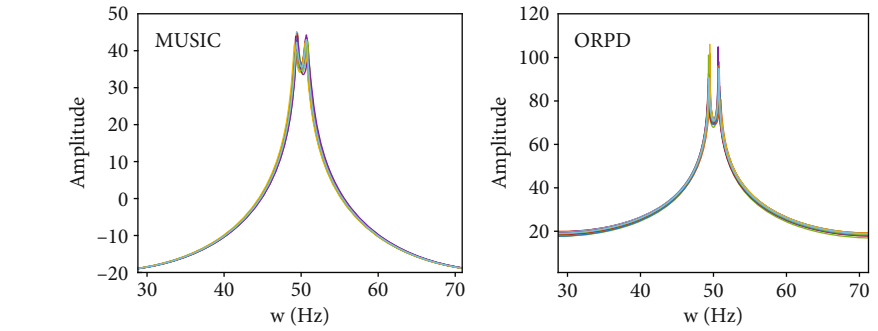

(a) Resolvability of signal $i_1(t)$

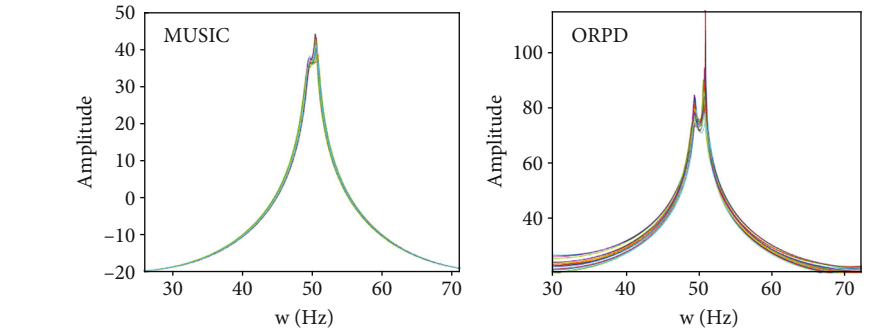

(b) Resolvability of signal $i_2(t)$

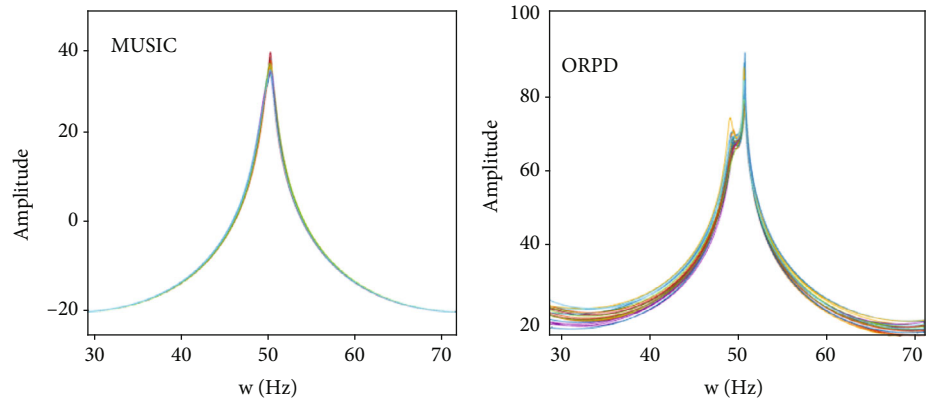

(c) Resolvability of signal $i_3(t)$

Figure 1: Comparison of the resolvability between MUSIC with ORPD algorithms.

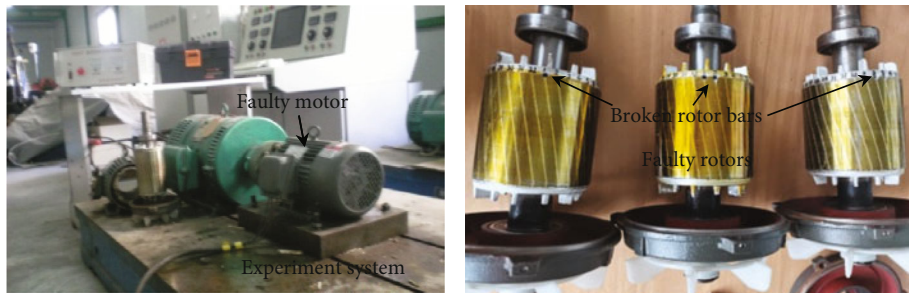

Figure 2: Experimental test bench and faulty rotors.

components according to the eigenvalues of the covariance matrix, and the possible pseudo-peak generated by ORPD algorithm are also avoided to the maximum extent. After the preprocessing of the stator current signal, the characteristic frequencies are obtained applying the ORPD algorithm, and the amplitude of the frequencies is estimated by LS algorithm. Finally, diagnosis decision is made based on frequency and amplitude estimation results.

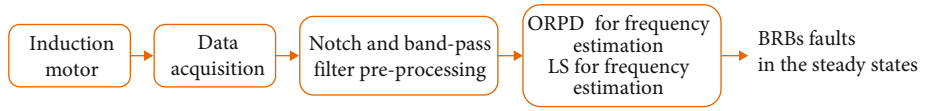

Figure 3: Proposed fault detection methodology, based in the use of the ORPD techniques.

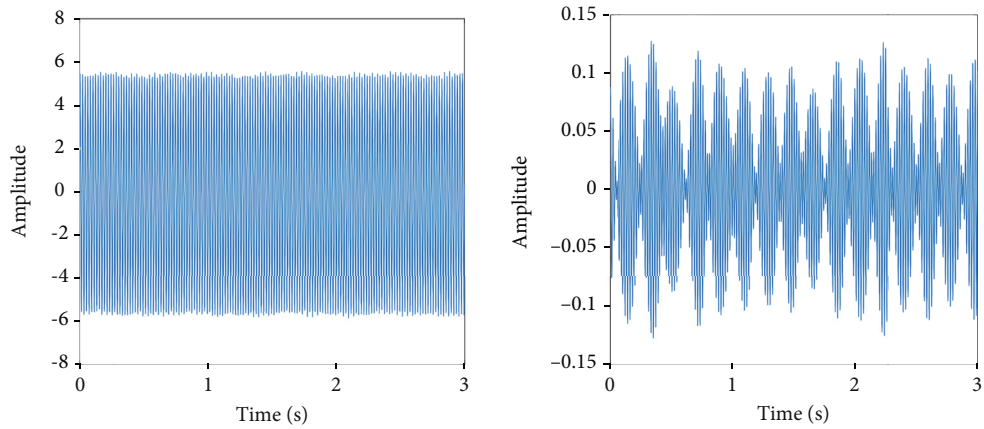

Figure 4: Time domain waveform of original stator current signal and preprocessed signal.

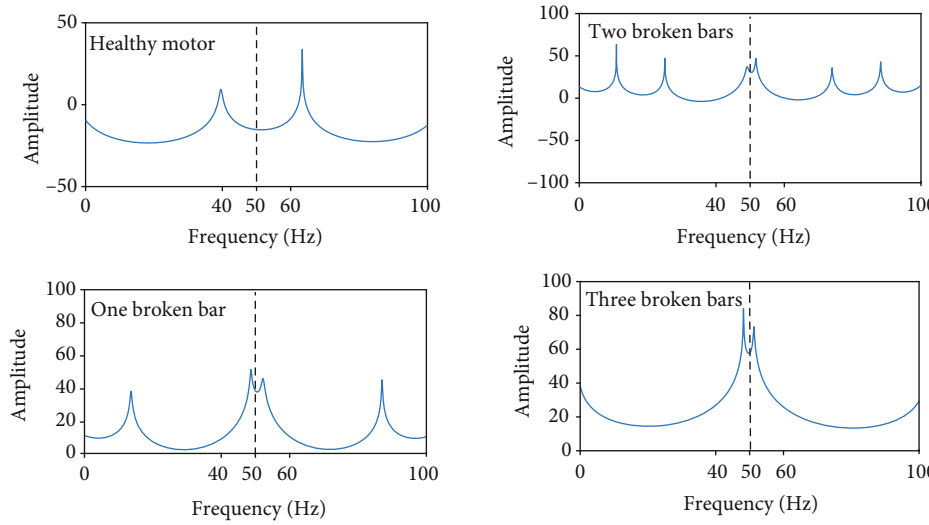

Figure 5: Comparison of ORPD current pseudo-spectra between the healthy and faulty machine with different severity.

Table 1: Parameter estimation results with the healthy and faulty machine with different severity using ORPD algorithm.

Fault type	Characteristics of the component	Theoretical value	Frequency estimation	Amplitude estimation
0	$(1-2s)f$	—	—	—
	$(1+2s)f$	—	—	—
1 broken rotor bar	$(1-2s)f$	48.7	48.66	0.019
	$(1+2s)f$	51.3	51.36	0.014
2 broken rotor bars	$(1-2s)f$	48.7	48.71	0.025
	$(1+2s)f$	51.3	51.32	0.021
3 broken rotor bars	$(1-2s)f$	48.7	48.70	0.035
	$(1+2s)f$	51.3	51.30	0.028

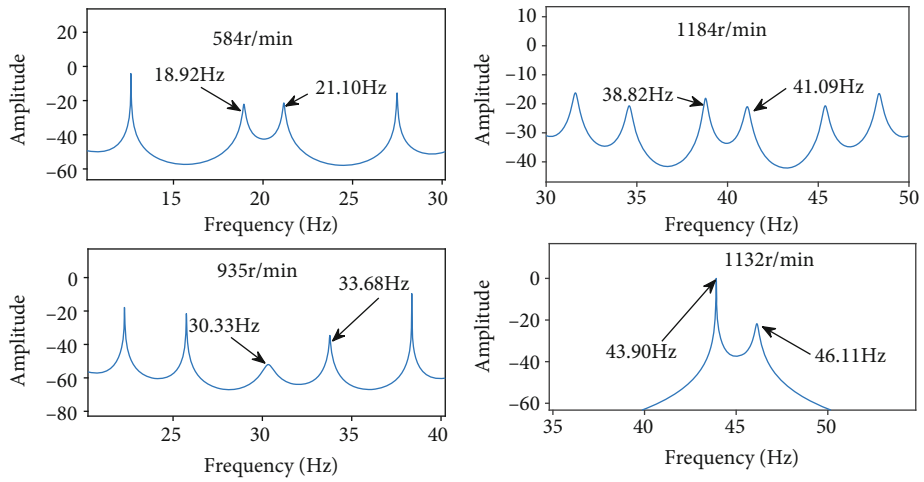

Figure 6: ORPD current pseudo-spectra of faulty induction motor with different power supply frequencies.

Table 2: Parameter estimation results with the faulty machine at different power supply frequencies using ORPD algorithm.

Power frequency (Hz)	Speed (r/min)	Characteristic component	Theoretical value	Frequency estimation	Amplitude estimation
20	584	$(1-2s)f$	18.92	18.92	0.036
		$(1+2s)f$	21.08	21.10	0.029
32	935	$(1-2s)f$	30.33	30.33	0.513
		$(1+2s)f$	33.67	33.68	0.462
40	1184	$(1-2s)f$	38.93	38.82	0.031
		$(1+2s)f$	41.07	41.09	0.027
45	1132	$(1-2s)f$	43.83	43.90	0.044
		$(1+2s)f$	46.17	46.11	0.039

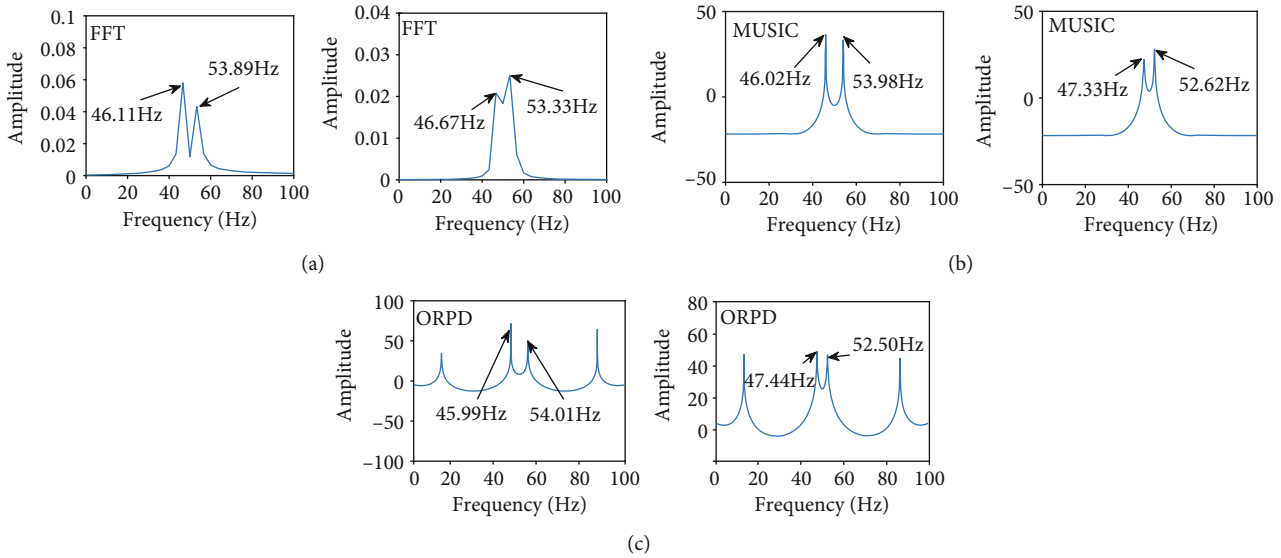

Figure 7: Comparison of FFT spectra with MUSIC and ORPD pseudo-spectra of faulty motor with different load levels (M =100, N =600). Left: 75% load, right: 50% load.

Table 3: Parameter estimation results of the faulty machine with different load levels using FFT, MUSIC, and ORPD algorithms.

Speed (r/min)	Characteristic component	Reference value	Estimated value		
			FFT	MUSIC	ORPD
1484	$(1-2s)f$	49	—	—	49.13
	A_1	0.021	—	—	0.017
	$(1+2s)f$	51	—	—	51.07
	A_2	0.016	—	—	0.012
1482	$(1-2s)f$	48.8	—	—	48.88
	A_1	0.028	—	—	0.025
	$(1+2s)f$	51.2	—	—	51.23
	A_2	0.020	—	—	0.020
1479	$(1-2s)f$	48.6	—	48.60	48.57
	A_1	0.044	—	0.045	0.044
	$(1+2s)f$	51.4	—	51.53	51.44
	A_2	0.038	—	0.035	0.036
1460	$(1-2s)f$	47.4	47.51	47.33	47.44
	A_1	0.102	0.108	0.108	0.107
	$(1+2s)f$	52.6	54.24	52.62	52.50
	A_2	0.087	0.099	0.090	0.091
1440	$(1-2s)f$	46.0	46.11	46.02	45.99
	A_1	0.123	0.113	0.120	0.121
	$(1+2s)f$	54.0	53.89	53.98	54.01
	A_2	0.101	0.107	0.105	0.105

4. Experimental Results

The original stator current signals of healthy and faulty motors were pretreated with the same band-pass and notch filtering. According to different analysis requirements, 1 s samples were randomly selected from the pretreated data for analysis. Figure 4 shows the time domain waveform of the stator current signal of a motor with 1 broken rotor bar fault and the signal after filtering and pretreatment.

4.1. Validation of Diagnostic Ability of ORPD Method

4.1.1. Diagnostic Ability of Power Supply Motor with Different Fault Severity. When the motor runs under low load, the stationarity of the stator current signal is easily affected by load fluctuation. At the same time, the fault characteristics are weak and gradually approaching with the load reduction. These factors put forward higher requirements for the short-time data diagnosis ability and frequency resolution of the algorithm. Therefore, the data of the healthy motor, 1, 2, and 3 broken rotor bars motors at low load (25% rated load, speed $n=1480$ r/min) were randomly selected for analysis to verify the diagnostic performance of the ORPD algorithm. Data length $N=600$ for experimental analysis. As can be seen from the ORPD spectrum of the healthy motor and the fault motor shown in Figure 5, for the healthy motor, there are no spectrum peaks on both sides of the 50 Hz dotted line in the spectrum, and only two spectrum peaks appear in the frequency band other than 40 Hz to 60 Hz. Obviously, these two spectrum peaks can be identified as pseudo peaks.

For the motors with 1-3 broken rotor bars, two spectrum peaks with equal distance distribution appear in a very small range on both sides of the 50 Hz dotted line. According to the frequency corresponding to the spectral peak position, it is found that the estimated frequency is consistent with the theoretical value, which indicates that ORPD algorithm can accurately estimate the fault characteristic frequency and judge the motor fault state based on it. Using Equation (15), the amplitude estimation obtained from the frequency estimation is shown in Table 1. It can be seen that the amplitude of the motor with different severity is significantly different, reflecting the actual situation that the severity is gradually increasing. It is shown that the proposed method can accurately diagnose the broken rotor bar fault and judge the severity of the fault. Compared with previous methods [11, 16, 19], the fault can be determined in only 1 s in this paper, and the diagnosis scope is extended to low load operation, indicating that the proposed method has advantages in short-time data diagnosis and resolution.

4.1.2. Diagnostic Ability under Different Power Supply Frequencies. When the motor is powered by a frequency converter, the noise component in the current signal increases significantly due to the influence of switching noise in the frequency converter. In low-frequency operation under speed regulation, the power frequency and motor speed decrease simultaneously, resulting in extremely weak fault characteristics. These factors not only lead to the reduction of SNR and difficulty in feature recognition but also make the diagnosis results susceptible to load fluctuations. Power supply frequencies are randomly set as 20 Hz, 32 Hz, 40 Hz, and 45 Hz, data time is 1 s, sample number $N=600$. The analysis results are shown in Figure 6, and Table 2 shows that the proposed method can still accurately identify the fault characteristics of broken rotor bars in frequency conversion power supply mode.

4.2. Performance Comparison of ORPD, MUSIC, and FFT Algorithms. FFT is a classical spectral estimation method; OPRD and MUSIC are high-resolution parameter estimation methods. In this section, based on the experimental data of three broken rotor bars motor under different load operation conditions, the short-time data diagnosis ability and anti-interference ability of ORPD, MUSIC, and FFT methods are compared, and the frequency resolution and operation performance of OPRD and MUSIC methods are compared.

4.2.1. Comparison of Short-Time Data Diagnostic Ability. The data of the motor at 75%, 50%, 23%, and 20% rated load were randomly selected for analysis, and the data time was 1 s. Figure 7 shows FFT spectrum, MUSIC and ORPD pseudo-spectra under 75% and 50% rated load. As can be seen from Figure 7, when FFT is used for spectrum analysis, two spectral peaks of characteristic frequency can still be

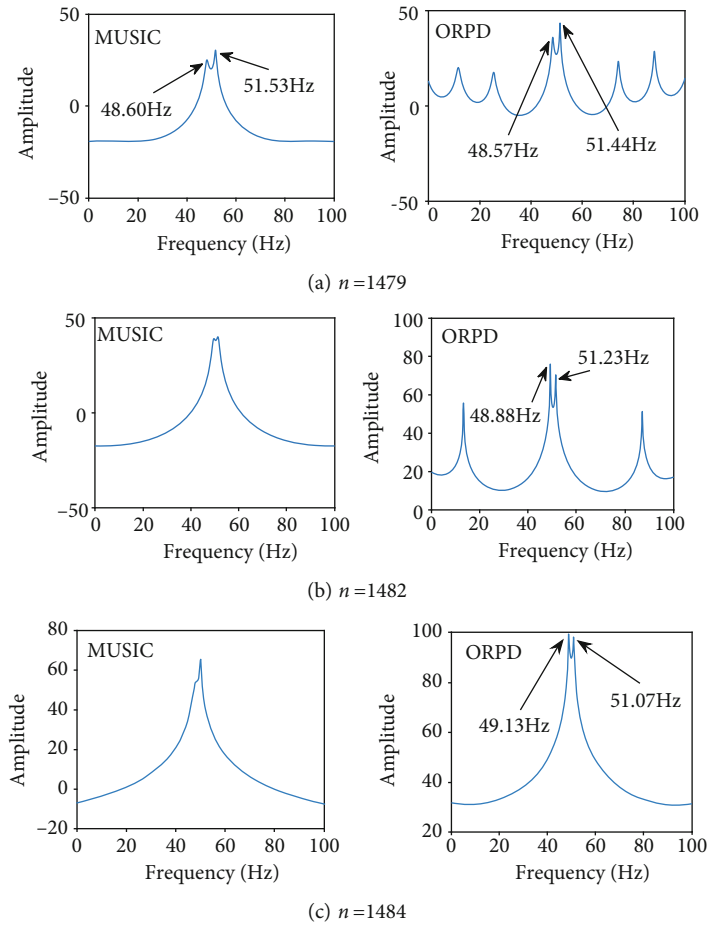

Figure 8: Comparison of the resolution performance between MUSIC with ORPD of faulty motor with lower load levels.

Table 4: Comparison of the number of successful resolution times for different data lengths with FFT, MUSIC, and ORPD algorithms.

Data length	The number of successful resolution times		
	FFT	MUSIC	ORPD
400	0	2	15
500	0	25	40
600	0	26	45
700	0	40	56
800	0	45	60
900	0	50	80
1000	0	60	90
1100	0	80	95
1200	10	95	100
1300	50	96	100
1400	81	96	100
1500	90	97	100
1600	95	99	100
1700	100	100	100

distinguished under 75% rated load, but it is difficult to distinguish under 50% rated load, indicating that FFT cannot be used for fault diagnosis of short-time data. In contrast, due to the long distance between the left and right characteristic frequency components, the ORPD and MUSIC algorithm can estimate the characteristic frequency accurately under 75% and 50% rated load, and there is no difference in the resolution between the two algorithms (shown in Table 3).

In order to further compare the fault diagnosis performance of ORPD and MUSIC algorithm under low load operation of motor, the load was adjusted randomly to make the motor run at 1479 r/min, 1482 r/min, and 1484 r/min, and the data analysis conditions were the same as above. As can be seen from Figure 8 and Table 3, when the load is low (n =1479 r/min), the estimated value of characteristic frequency can also be obtained based on MUSIC algorithm. However, as the load decreases (speed n increases), the spectral peak becomes unclear, and the estimated value of frequency obtained based on the pseudo-spectral peak differs greatly from the real value until it cannot be estimated. In contrast, the spectral peak of ORPD algorithm is always clear, and the estimated frequency and amplitude obtained from the spectral peak are very close to the real value, and the resolution of ORPD algorithm is significantly better than that of MUSIC algorithm.

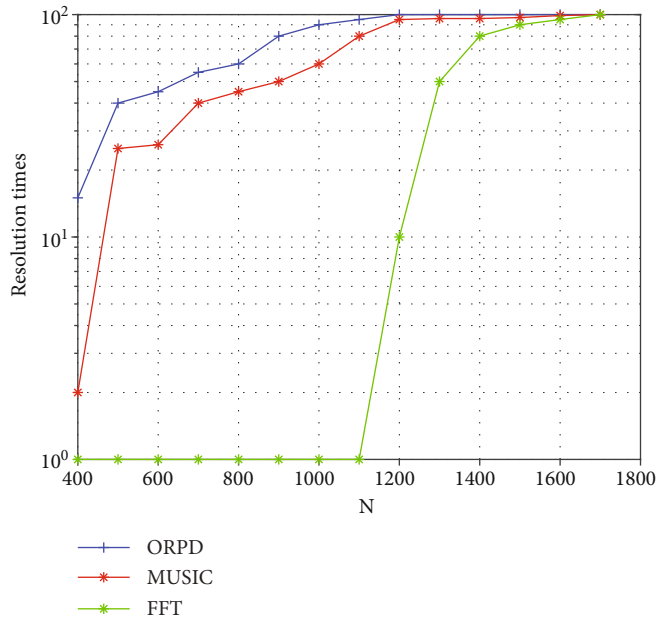

Figure 9: Influences of data lengths on diagnostic performance of FFT, MUSIC, and ORPD algorithms.

The results show that the frequency resolution and diagnostic performance of ORPD and MUSIC are significantly higher than that of FFT when the motor is running under 50% rated load for short-time data of 1 s. As the load decreases, when the motor runs under low load, the resolution of MUSIC decreases significantly and even fails. In contrast, ORPD consistently maintains high-frequency resolution and can identify fault features even at 20% load rating, demonstrating superior short-time data diagnosis ability.

4.2.2. Comparison of Anti-Interference Ability. In practical application, the longer the signal data used for diagnostic analysis, the more likely the diagnosis result is affected by data noise, and ambiguity frequency may occur in the case of load fluctuation, increasing the risk of misdiagnosis. Therefore, the length of data used for diagnostic analysis is an important indicator to measure the anti-interference performance of a diagnostic method. In order to compare the diagnostic performance of ORPD, MUSIC, and FFT algorithms in different data lengths, several data segments of different lengths were selected for statistical analysis. During the analysis, the matrix dimension $M=100$, the motor speed $n=1482$ r/min under low load, and the data length N ranged from 400 to 1700 sampling points. Under certain conditions of N, take different data to do 100 independent experiments.

The frequency error UE is defined as shown in Equation (19), where f_{est} is the estimated frequency value and f_{true} is the theoretical value calculated according to slip s.

$$UE = |f_{est} - f_{true}|. \tag{19}$$

Under the condition of $UE < 0.3$, the number of successful resolution times of various algorithms was counted, and the statistical results are shown in Table 4 and Figure 9.

As can be seen from Table 4 and Figure 9, as the length of signal data N increases gradually, the number of successful resolution times of all algorithms increases gradually. However, under the same data length, the number of successful resolution times of ORPD and MUSIC algorithm is significantly higher than FFT algorithm, and ORPD is always higher than MUSIC algorithm. This shows that ORPD algorithm has obvious advantages in short-time data diagnosis and therefore has better anti-interference ability than MUSIC and FFT algorithms.

4.2.3. Comparison of Performance between ORPD and MUSIC Methods. The frequency resolution and operation time of ORPD and MUSIC methods depend on the dimension of self-correlation matrix M ($M \le N$). If M is too small, the characteristic frequency cannot be identified. If M is too large, too much computing resources are occupied.

In order to compare the performance of the two methods, the speed $n=1482$ r/min was set when the motor was running under low load, and the corresponding 20 different data with length $N=600$ were taken. Independent experiments were repeated when $M=200$, 150, and 100, and the spectra were recorded and the data were analyzed. The simulation operation time corresponding to $M=200$, 150, and 100 is 43 s, 31 s, and 22 s, respectively. The simulation spectra are shown in Figure 10. As can be seen from Figure 10, with the decrease of M, the resolution of MUSIC algorithm will gradually decline, but the resolution of ORPD remains unchanged.

This means that in order to maintain the same frequency resolution, MUSIC requires an increase in the dimension of matrix M, resulting in an increase in computing time and hardware requirements. In contrast, ORPD is more convenient for system development and integration due to its advantages in computing performance.

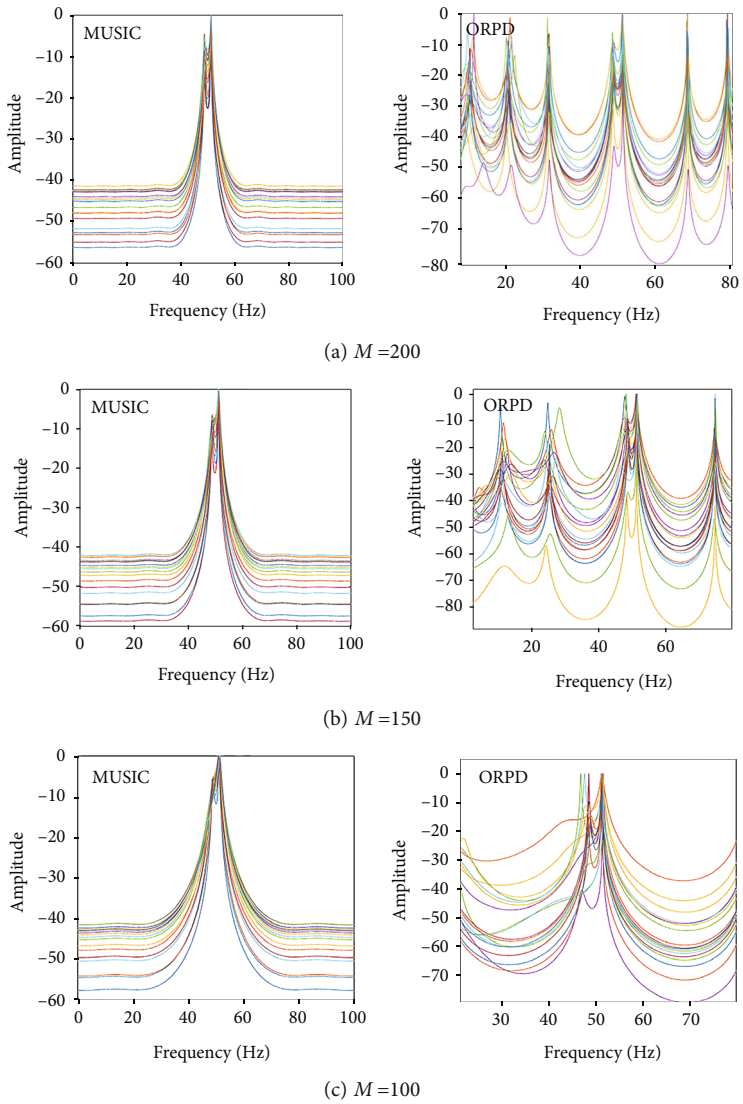

Figure 10: Influences of dimension of the autocorrelation matrix M on diagnostic performance of MUSIC and ORPD algorithms.

5. Conclusions

Theoretical and simulation analyses show that the ORPD algorithm has the best frequency resolution performance under the condition of the prior information of the predicted parameters. The characteristic frequencies of broken rotor bar faults are symmetrically distributed on both sides of the fundamental frequency f_s. Using this prior information, by constructing a weighted matrix with the lowest SNR resolution threshold, ORPD algorithm with the best frequency resolution performance can be developed to estimate the characteristic frequencies of broken rotor bar faults in the stator current spectrum.

Experimental results show that due to its high-frequency resolution, the proposed method has good diagnostic ability for motors with different fault severity of power frequency and frequency conversion power supply. When the motor runs at low load and frequency conversion power supply at low-frequency band, the SNR is low and the fault characteristics are susceptible to load fluctuation. In this case, the method presented in this paper still has strong diagnostic ability and can diagnose the broken rotor bar fault under the short-time data condition of 1 s. Compared with FFT and MUSIC methods, the proposed method has obvious advantages in short-time data diagnosis ability, anti-interference ability, and computing performance, so it is convenient for the development of portable diagnosis device and the integration of diagnosis system.

The ORPD algorithm adopted in this paper is better than FFT and MUSIC algorithm in frequency resolution, but it still has shortcomings in accuracy. In addition, the accuracy of frequency estimation is affected by signal preprocessing technology, which will be the focus of the next stage of research.

Data Availability

The data used to support the findings of this study are included within the article.

Conflicts of Interest

The authors declare that they have no competing interest.

Acknowledgments

This work was funded by the National Natural Science Foundation of China (52007078) and the Research Project of Education Department of Liaoning Province (2019LNJC16).

References

[1] H. Y. Li, G. Feng, D. Zhen, F. Gu, and A. D. Ball, "A normalized frequency-domain energy operator for broken rotor bar fault diagnosis," *IEEE Transactions on Instrumentation and Measurement*, vol. 70, no. 1, pp. 1–10, 2021.

[2] D. B. de Deus, C. A. Sobrinho, F. A. Belo, A. V. Brito, J. G. de Souza Ramos, and A. C. Lima-Filho, "Density of maxima approach for broken bar fault diagnosis in low slip and variable load conditions of induction motors," *IEEE Transactions on Instrumentation and Measurement*, vol. 69, no. 12, pp. 9797–9804, 2020.

[3] J. Antonino-Daviu, "Electrical monitoring under transient conditions: a new paradigm in electric motors predictive maintenance," *Applied Sciences*, vol. 10, no. 17, p. 6137, 2020.

[4] A. Kabul and A. Unsal, "Detection of broken rotor bars of induction motors based on the combination of Hilbert envelope analysis and Shannon entropy," *Tm-Technisches Messen*, vol. 88, no. 1, pp. 45–58, 2021.

[5] D. A. Elvira-Ortiz, D. Morinigo-Sotelo, A. L. Zorita-Lamadrid, R. A. Osornio-Rios, and R. J. Romero-Troncoso, "Fundamental frequency suppression for the detection of broken bar in induction Motors at low slip and frequency," *Applied Sciences*, vol. 10, no. 12, p. 4160, 2020.

[6] J. G. Chen, N. Hu, L. Zhang, L. Chen, B. Wang, and Y. Zhou, "A method for broken rotor bars diagnosis based on sum-of-squares of current signals," *Applied Sciences*, vol. 10, no. 17, p. 5980, 2020.

[7] W. F. Godoy, I. N. da Silva, A. Goedtel, R. H. C. Palácios, and T. D. Lopes, "Application of intelligent tools to detect and classify broken rotor bars in three-phase induction motors fed by an inverter," *IET Electric Power Applications*, vol. 10, no. 5, pp. 430–439, 2016.

[8] O. E. Hassan, M. Amer, A. K. Abdelsalam, and B. W. Williams, "Induction motor broken rotor bar fault detection techniques based on fault signature analysis - a review," *IET Electric Power Applications*, vol. 12, no. 7, pp. 895–907, 2018.

[9] F. Filippetti, A. Bellini, and G. A. Capolino, "Condition monitoring and diagnosis of rotor faults in induction machines: state of art and future perspectives," in *2013 IEEE Workshop on Electrical Machines Design, Control and Diagnosis (WEMDCD)*no. 4, pp. 196–209, Paris, France, 2013.

[10] H. Henao, G. A. Capolino, M. Fernandez-Cabanas et al., "Trends in fault diagnosis for electrical machines: a review of diagnostic techniques," *IEEE Industrial Electronics Magazine*, vol. 8, no. 2, pp. 31–42, 2014.

[11] S. H. Kia, H. Henao, and G. A. Capolino, "A high-resolution frequency estimation method for three-phase induction machine fault detection," *IEEE Transactions on Industrial Electronics*, vol. 54, no. 4, pp. 2305–2314, 2007.

[12] M. E. H. Benbouzid, M. Vieira, and C. Theys, "Induction motors' faults detection and localization using stator current advanced signal processing techniques," *IEEE Transactions on Power Electronics*, vol. 14, no. 1, pp. 14–22, 1999.

[13] L. A. Pereira, D. Fernandes, D. S. Gazzana, F. B. Libano, and S. Haffner, "Application of the Welch, Burg and MUSIC methods to the detection of rotor cage faults of induction motors," in *2006 IEEE/PES Transmission & Distribution Conference and Exposition: Latin America*, Caracas, Venezuela, 2006.

[14] V. Choqueuse, M. Benbouzid, and J. F. Charpentier, "Induction machine fault detection enhancement using a stator current high resolution spectrum," in *IECON 2012-38th Annual Conference on IEEE Industrial Electronics Society*, Montreal, QC, Canada, 2012.

[15] J. Wang, Y. Xue, and L. Zhigang, "Equivalence of DOA and frequency estimation," *Journal of Yanshan University*, vol. 28, no. 1, pp. 29–32, 2004.

[16] F. Fang, Y. Shi-yuan, and H. Xin-guo, "Rotor fault feature extraction of motor faults of induction motor based on a modified music method," *Zhongguo Dianji Gongcheng Xuebao(-Proceedings of the Chinese Society of Electrical Engineering)*, , no. 30, pp. 72–76, 2007.

[17] A. Naha, A. K. Samanta, A. Routray, and A. K. Deb, "Determining autocorrelation matrix size and sampling frequency for MUSIC algorithm," *IEEE Signal Process*, vol. 22, no. 8, pp. 1016–1020, 2015.

[18] M. Wax and T. Kailath, "Detection of signals by information theoretic criteria," *Signal Processing*, vol. 33, no. 2, pp. 387–392, 1985.

[19] X. Boqiang, S. Liling, and L. Heming, "A detection method for broken rotor bar fault in induction motors based on multiple signal classification and pattern search algorithm," *Zhongguo Dianji Gongcheng Xuebao(Proceedings of the Chinese Society of Electrical Engineering)*, , no. 30, pp. 72–76, Chinese Society for Electrical Engineering, 2007.

[20] X. Gao, Z. Chengyun, and C. Hongsen, "Estimation for signals DOA by modified MUSIC algorithm," *Journal of System Simulajion*, vol. 17, no. 1, pp. 233–245, 2005.

[21] S. U. Pillai and B. H. Kwon, "Performance analysis of MUSIC-type high resolution estimators for direction finding in correlated and coherent scenes," *IEEE Transactions on Acoustics, Speech, and Signal Processing*, vol. 37, no. 8, pp. 1176–1189, 1989.

[22] M. Kaveh and A. J. Barabell, "The statistical performance of the MUSIC and the minimum-norm algorithms in resolving plane waves in noise," *IEEE Transactions on Acoustics, Speech, and Signal Processing*, vol. 34, no. 2, pp. 331–341, 1986.

[23] J. Luo and Z. Bao, "The resolution performance of eigenstructure approach," *Journal of Electronics*, vol. 13, no. 4, p. 337, 1991.

[24] D. Zheng, Z. Zifa, and S. Yingchun, "Performance comparison of several eignstructure algorithms for estimation of DOA," *Shipboard Electronic Counter measure*, vol. 29, no. 1, pp. 30–34, 2006.

[25] Z. D. Cheng, J. Q. Luo, X. Fan, and D. H. Ma, "Effect of power difference of two signal sources on resolving performance of MUSIC algorithm," *Journal of Electronics and Information Technology*, vol. 30, no. 5, pp. 1088–1091, 2008.